Geophysical Research Letters

RESEARCH LETTER
10.1029/2018GL080958

How Is Meridional Coherence Maintained in the Lower Limb of the Atlantic Meridional Overturning Circulation?

Sijia Zou[1], **M. Susan Lozier**[1], **and Martha Buckley**[2]

[1]Division of Earth and Ocean Sciences, Nicholas School of the Environment, Duke University, Durham, NC, USA, [2]Department of Atmospheric, Oceanic, and Earth Sciences, George Mason University, Fairfax, VA, USA

Abstract Despite a strong focus on latitudinal continuity of the Atlantic Meridional Overturning Circulation (AMOC) variability, transport continuity in different layers that constitute the AMOC lower limb has received considerably less attention. In this study, we investigate the transport connectivity of Upper North Atlantic Deep Water (UNADW) and Lower NADW (LNADW), with both defined by density. Using two ocean circulation models and an ocean reanalysis, we find that subpolar-originated transport anomalies, particularly for UNADW, do not propagate to the subtropics over a period of five decades. We also find that transports in both layers are linked to AMOC at subpolar latitudes, yet only LNADW transport shows linkage to AMOC in the subtropical gyre. Thus, latitudinal AMOC continuity is likely unrelated to transport continuity in any single layer, but rather a result of connection between subpolar-AMOC and subtropical-LNADW transport. An exception to this generalization is possible with strong LNADW transport events.

Plain Language Summary The importance of studying the Atlantic Meridional Overturning Circulation (AMOC), characterized as northward flowing upper waters and southward flowing deep waters, lies in its significant impacts on climate. The production of deep waters in the subpolar/subarctic North Atlantic (i.e., North Atlantic Deep Water or NADW) has been assumed to create coherent NADW transport changes across a range of latitudes. Such latitudinal transport coherence is thought to create a latitudinal coherent AMOC. However, though AMOC transport coherence has been widely discussed, no study to date has explored the latitudinal coherence of NADW or its relationship with AMOC. This study aims to fill this gap. We find that transport anomalies of NADW since the 1960s, specified by different density class, do not propagate coherently from the subpolar gyre to the subtropical gyre, suggesting that latitudinal AMOC coherence is unlikely achieved through coherent transport of these deep waters. Our study challenges the paradigm that the subtropical AMOC is strongly impacted by deep water production in the subpolar gyre and highlights the importance of local forcing on AMOC variability. Both results have implications for the ocean's role in climate variability.

Key Points:
- Deep water transport anomalies in the AMOC lower limb generally lack meridional coherence
- The meridional coherence in AMOC lower limb is a result of gyre-dependent relationships between deep water transport and the AMOC

Supporting Information:
- Supporting Information S1

Correspondence to:
S. Zou,
sijia.zou@duke.edu

Citation:
Zou, S., Lozier, M. S., & Buckley, M. (2019). How is meridional coherence maintained in the lower limb of the Atlantic Meridional Overturning Circulation? *Geophysical Research Letters*, *46*, 244–252. https://doi.org/10.1029/2018GL080958

Received 16 OCT 2018
Accepted 11 DEC 2018
Accepted article online 14 DEC 2018
Published online 3 JAN 2019

1. Introduction

The Atlantic Meridional Overturning Circulation (AMOC) is characterized by northward flowing upper layer waters and southward flowing deep waters. Its strength at specific latitudes is quantified as the total northward upper layer transport (e.g., Cunningham et al., 2007; Li et al., 2017). Models have revealed a meridional coherence of AMOC variability in response to the production of Labrador Sea Water (LSW; Biastoch et al., 2008; Delworth et al., 1993; Polo et al., 2014; Yeager & Danabasoglu, 2014; Zhang, 2010). It is generally assumed that this meridional coherence is achieved via the export of subpolar-originated deep waters to lower latitudes, yet a few recent studies have cast doubt on this supposition.

From an analysis of moored current meter data over two periods 1993–1995 (strong LSW production) and 1999–2001 (weak LSW production), Schott et al. (2004) find no causal linkage between LSW production and deep boundary current transports east of the Grand Banks. Instead, the authors conclude that the deep transports in this region are more closely related to North Atlantic Current variability. By focusing only on boundary current transports, this study does not account for the transport of waters carried equatorward in the lower AMOC limb by interior pathways (Bower et al., 2009; Gary et al., 2012; Lozier, 1997), so it is possible that this omission impacts their conclusion.

A second study, based on an eddy-permitting ocean-general circulation model, explores the relationship between LSW production and its Lagrangian export to the subtropical gyre on interannual to decadal time scales (Zou & Lozier, 2016). The authors find that an anomalously large (small) production of LSW does not result in an increased (decreased) export to the subtropical gyre in subsequent years, suggesting a negligible or at best modest impact of LSW production on downstream LSW transport. This finding is attributed to the strong recirculation of LSW within the subpolar gyre (Gary et al., 2012; Lavender et al., 2005) and the presence of interior pathways from the subpolar to the subtropical gyre that act as a strong filter for LSW production signals.

Also related to the linkage between the AMOC and deep water transport are recent studies based on observations at the RAPID array (26.5°N) that have revealed the dominance of local forcing on deep water transport variability. AMOC variability on interannual to semi-decadal time scales at this subtropical latitude is dominated by wind-driven upper ocean transport (Cabanes et al., 2008; Roberts et al., 2013; Zhao & Johns, 2014). Transport in the lower AMOC limb has, as expected, an in-phase response to these upper limb changes: as the upper limb increases or decreases its northward flow, the lower limb's southward flow responds in kind. Interestingly, this mass compensation is largely contained within the Lower North Atlantic Deep Water (LNADW, 3,000–5,000 m) layer rather than the Upper North Atlantic Deep Water (UNADW, 1,000–3,000 m) layer (Figure S1 in the supporting information; Frajka-Williams et al., 2016; McCarthy et al., 2012), the latter of which is generally understood to contain subpolar-originated LSW layer water.

Taken together, these studies raise questions about the role of the deep waters in maintaining the AMOC meridional connectivity. Specifically, they raise questions about (1) the extent to which deep water transport anomalies from the subpolar gyre impact transport anomalies downstream within the same density class and (2) the extent to which local AMOC variability is linked to deep water transport variability. To our knowledge, no study to date has explored these two questions. To address this gap, we utilize output from eddy-resolving/permitting ocean circulation models and an ocean reanalysis. This choice permits an exploration of connectivity on longer time scales and over a broader spatial domain than available observations allow.

2. Data

For our study, we use the eddy-resolving (1/12°) member of the Family of Linked Atlantic Models Experiment (FLAME; Biastoch et al., 2008; Böning et al., 2006), forced with monthly anomalies of National Centers for Environmental Prediction/National Center for Atmospheric Research reanalysis data set (Kalnay et al., 1996) superimposed on European Centre for Medium-Range Weather Forecasts climatological forcing to create a hindcast data set from 1990 to 2004. The model domain spans from 18°S to 70°N on a Mercator grid and has 45 z coordinate levels in the vertical, with spacing increasing from 10 m near the surface to 250 m in the deep ocean. Monthly temperature, salinity, and velocity fields, averaged from the 3-day output, are used in this study. For further model details and for model validations of North Atlantic deep water transport, the reader is referred to Gary et al. (2011) and Zou et al. (2017).

We also use ORCA025, a global ocean/sea ice model implemented on a quasi-isotropic tripolar grid at eddy-permitting resolution (1/4°) based on the NEMO (Nucleus for European Modeling of the Ocean) system (Barnier et al., 2006; The DRAKKAR group, 2007). ORCA025 has 46 vertical layers, with vertical grid spacing increasing from 6 m near the surface to 250 m at the bottom. Horizontal resolution increases with latitude, with the coarsest resolution (27.75 km) at the equator. ORCA025 is forced with European Remote Sensing Satellite (ERS) Scatterometer data and National Centers for Environmental Prediction/National Center for Atmospheric Research reanalysis data, and an empirical bulk parameterization (Goosse, 1997) is used to compute the surface fluxes. Monthly data, averaged from the 5-day output from 1961 to 2004, is used in this study. Additional details and model validations can be found in Barnier et al. (2006), Gary et al. (2011), and Zou and Lozier (2016).

Finally, we use the Simple Ocean Data Assimilation (SODA2.2.4) reanalysis in our study, which has been shown to compare favorably to available observations of deep water transports and the AMOC (Tett et al., 2014). SODA, based on an ocean circulation model (POP2.x) that is forced with the 20th Century Reanalysis project (20CRv2) atmospheric data product, sequentially assimilates observations from

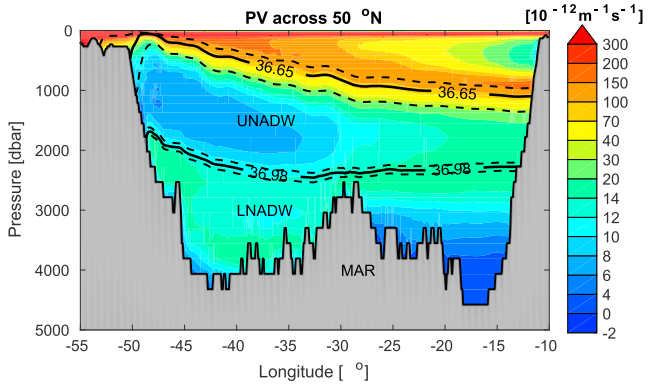

Figure 1. Identification of UNADW and LNADW in σ_2 space at 50°N in FLAME. The upper bound of UNADW is denoted by $\sigma_2^{\max}(50^{\circ}\mathrm{N})$, the time mean of which is 36.65 kg/m^3 (solid black line), with a minimum/maximum of 36.47/36.80 kg/m^3 (dashed lines). The lower bound of UNADW is denoted by the isopycnal of 36.98 kg/m^3, which is determined by the climatological PV field ($\leq 10 \times 10^{-12}$ m$^{-1} \cdot$ s^{-1}, shown in background color). The standard deviation of this lower bound, determined by annually varying low PV, is also shown as dashed lines, with a minimum of 36.97 kg/m^3 and a maximum of 36.99 kg/m^3. Sensitivity tests show robust results using different choices of the separating isopycnals that lie within one standard deviation of the climatology. See Figures S2 and S3 for similar plots in ORCA and SODA. UNADW = Upper North Atlantic Deep Water; LNDW = the Lower North Atlantic Deep Water; PV = potential vorticity.

World Ocean Database and the International Comprehensive Ocean-Atmosphere Data Set (Carton & Giese, 2008). The model has a horizontal resolution of 0.25° × 0.4° on average and has 40 vertical levels. Data used in this paper are the monthly averages mapped onto a uniform 0.5° × 0.5° × 40-level grid from 1961 to 2009. While ideally transports should be calculated using variables on the native model grid, these fields are not available for SODA 2.2.4. However, analyses with other models (e.g., ORCA025 and SODA3.7.1) generally show that interpolation errors affect mean transports rather than variability, which is our focus here.

3. Calculating AMOC and UNADW/LNADW Transport in Density Space

At each latitude (φ), AMOC strength is defined as the maximum of the overturning streamfunction (Ψ) in σ_2 space,

$$\begin{aligned} \mathrm{AMOC}(\varphi, \mathrm{t}) &= \max\Psi(\varphi, \sigma_2, \mathrm{t}) \\ &= \max\left[\int_{\sigma_2\mathrm{surface}}^{\sigma_2}\int_{x_w}^{x_e} v(\mathrm{x}, \varphi, \sigma_2, t)\mathrm{d}x\mathrm{d}\sigma_2\right]. \end{aligned} \quad (1)$$

Here $v(\mathrm{x}, \varphi, \sigma_2, t)$ is the meridional velocity in σ_2 space and x is longitude, with x_w and x_e denoting the westernmost and easternmost positions, respectively, of the ocean bottom at a particular σ_2 level. The AMOC strength, $\mathrm{AMOC}(\varphi, \mathrm{t})$, achieved at $\sigma_2 = \sigma_2^{\max}(\varphi, \mathrm{t})$, is calculated from monthly data at each latitude between [25°N, 53°N]. The results are then averaged annually and a linear trend is removed.

The UNADW layer is defined as the water directly below the time-varying isopycnal that separates the northward from the southward flow, that is, at $\sigma_2^{\max}(\varphi, \mathrm{t})$, and above an isopycnal that identifies the climatological LSW layer (with low potential vorticity, PV) from overflow waters in the subpolar gyre (Figures 1 and S2 and S3). When heading southward to the subtropical gyre, the low-PV characteristic of LSW is mostly lost, particularly in the basin interior. However, the majority of the LSW remains in the same density class, as shown by observed tracer fields (Gary et al., 2012) and by simulated Lagrangian studies (Gary et al., 2012; Zou & Lozier, 2016). As such, the UNADW layer defined above contains a large majority of the LSW exported into the subtropical gyre, but it also includes other intermediate waters that share the same density class. Both the time-varying UNADW upper bound ($\sigma_2^{\max}(\varphi, \mathrm{t})$) and the climatological PV-based lower bound are model specific.

The LNADW layer is defined as the layer below UNADW and above the ocean floor. Both UNADW and LNADW layers are dynamic, meaning that their thickness varies in time. The sum of transports in both layers constitute the transport in the entire AMOC lower limb, which equals the AMOC upper limb due to mass conservation. Transport time series for each layer are calculated at each latitude as the integrated transport across all longitudes over each layer's thickness, that is,

$$T(\varphi, t) = -\int_{\sigma_2\ \text{lower bound}}^{\sigma_2\ \text{upper bound}}\int_{x_w}^{x_e} v(\mathrm{x}, \varphi, \sigma_2, t)\mathrm{d}x\mathrm{d}\sigma_2. \quad (2)$$

With this sign convention, a southward flow will have a positive value of $T(\varphi, t)$. All time series are derived from monthly data, which are then averaged into annual means before the trend is removed.

This study is primarily based on the annual time series described above. We repeat our analysis in ORCA and SODA after applying a third-order 8-year Butterworth low-pass filter, as previous modeling studies have suggested that AMOC is more coherent on decadal time scales (e.g., Biastoch et al., 2008). The results based on these low-pass-filtered time series (see supporting information) are consistent with those from the annual (i.e., unfiltered) time series.

4. Results

4.1. Meridional Connectivity of AMOC Anomalies

The 15-year mean overturning stream function in density space in FLAME is shown in Figure 2a. Interestingly, two overturning cells with comparable strength are present, with one located in the subtropical gyre and the other at subpolar latitudes. The maximum of the subtropical cell is 20.6 Sv (1 Sv = 10^6 m^3/s) and the maximum of the subpolar cell is 19.3 Sv. The strength of the subpolar cell is significantly reduced when calculated in depth space (12.9 Sv), as pointed out by other studies (e.g., Zhang, 2010), due to strongly sloping isopycnals in that basin. The two-cell structure of the overturning stream function in density space is also present in ORCA and SODA (not shown). The maximum of the subtropical (subpolar) cell for ORCA is 14.5 Sv (16.6 Sv), and for SODA is 24.2 Sv (19.8 Sv). In this study, our main focus is on the consistency in the meridional connectivity across data sets, rather than on similarities/differences in AMOC magnitude and variability among data sets. Importantly, those differences do not impact the results of this study.

In all three data sets, the detrended AMOC shows intragyre in-phase variability in both the subpolar and the subtropical gyres, with a discontinuity at the gyre-gyre boundary (Figure 2b for FLAME; Figure S4a for ORCA025; Figure S5a for SODA). To further evaluate the downstream propagation of AMOC anomalies generated in the subpolar gyre, cross-correlation coefficients are calculated using the AMOC time series averaged over 52–53°N and the AMOC at other latitudes (Figures 3a–3c). In addition to the gyre-specific in-phase variability of AMOC, all models show a significant linkage between the subpolar and subtropical AMOCs, with the former leading by less than 4 years (consistent with Zhang, 2010). In the next sections, we examine this meridional connectivity in different vertical layers that constitute AMOC lower limb.

4.2. Meridional Connectivity of Transport Anomalies in UNADW/LNADW Layer

In general, both UNADW and LNADW transports show intragyre in-phase variability for both the subpolar and the subtropical gyres (Figures 2c and 2d for FLAME; Figures S4b and S4c for ORCA025; Figures S5b and S5c for SODA). However, whether the subpolar and the subtropical transports are connected is not easily assessed from these plots. Thus, to further investigate the meridional connectivity, we calculate cross-correlation coefficients between the UNADW transport time series averaged over 52–53°N and UNADW time series at other latitudes (Figures 3d–3f). At all subpolar latitudes, significant 0-lag correlations are present, indicating an in-phase gyre-scale variability. However, for all three models the positive correlations drop dramatically at the gyre-gyre boundary, indicating either that UNADW transport anomalies do not propagate to the subtropical gyre or that the propagated anomalies are too weak to impact local transport.

We conduct the same assessment for LNADW. In this case, significant correlations extend from the subpolar gyre to the subtropical gyre, with the former leading by less than 4 years (Figures 3g–3i). Such lagged meridional connectivity suggests the LNADW layer as a potential layer through which subpolar-originated AMOC anomalies travel to the subtropical gyre.

The meridional connectivity in this layer, however, appears contingent on the strength of the transport anomalies. For example, LNADW transport variability in both gyres in FLAME is dominated by strong anomalies in the 1990s (Figure 2d), which are also captured in ORCA025 (Figure S4c). These strong anomalies, which appear to originate in the subpolar gyre, exhibit a relatively coherent southward spreading compared to anomalies in other years, raising the possibility that the meridional connectivity of LNADW transport is maintained by these strong anomalies alone. The LNADW transport anomalies in SODA are generally weak in the subpolar gyre (Figure S5c), but relatively strong anomalies in the early 1980s also exhibit a stronger meridional connectivity compared to other time periods.

To test the impact of strong LNADW anomalies on the meridional connectivity, we recalculate the correlation between transport at 52–53°N and transport downstream within the LNADW layer in ORCA025 without the 1990s time series, and in SODA without the 1984–1988 time series (Figures 3j and 3k). Interestingly, no significant correlation (at positive lags) is observed south of 35°N. To ensure that this lack of correlation is due to the exclusion of the strong anomaly event instead of the shortening of the time series, we repeat the calculation with a time series that has the same temporal length but now includes the strong anomaly event (e.g., 1976–2004 for ORCA025). The cross-correlation map is very similar to Figures 3h and 3i.

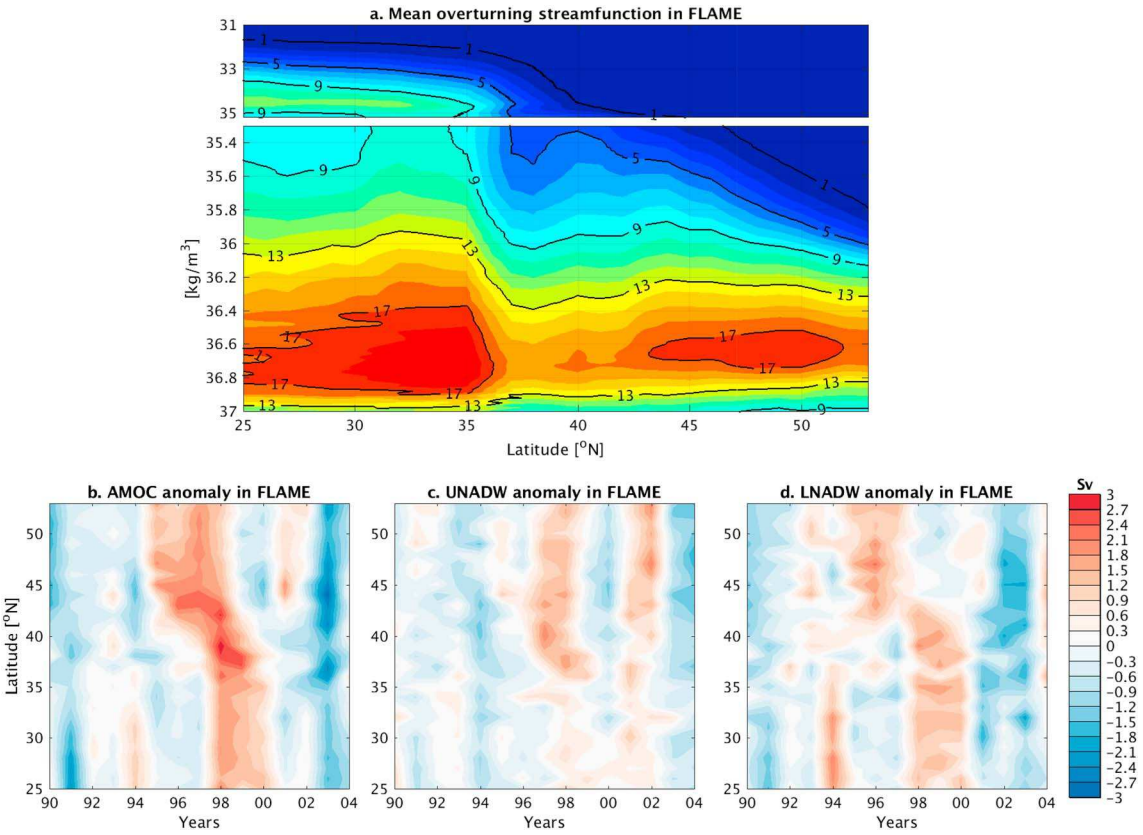

Figure 2. (a) Mean overturning stream function (unit: Sv) in density space from FLAME. The contour interval is 1 Sv. Hovmöller diagram of AMOC strength anomalies (b), UNADW transport anomalies (c), and LNADW transport anomalies (d) in FLAME. FLAME = Family of Linked Atlantic Models Experiment; UNADW = Upper North Atlantic Deep Water; LNADW = the Lower North Atlantic Deep Water; AMOC = Atlantic Meridional Overturning Circulation.

Collectively, the above analysis suggests that (1) an AMOC intergyre meridional connectivity is not maintained in the UNADW layer and (2) it can be achieved within LNADW layer, but only during periods with strong anomalies. It is worth noting that these conclusions remain consistent if we use low-pass-filtered time series (Figure S6).

One question that remains unanswered is whether the meridional connectivity in the LNADW layer is the only contributor to AMOC meridional coherence. The answer is no. If the periods with strong LNADW anomalies are excluded, the meridional coherence of AMOC is still present (Figure S7), indicating there is another mechanism responsible for AMOC inter-gyre connection. We turn to this dilemma in section 4.3 below.

4.3. Relationship Between AMOC Variability and Transport Variability in the UNADW/LNADW Layer

We now turn to the second part of our investigation, namely a study of the relationship between local (i.e., at the same latitude) AMOC variability and local deep water transport variability. In the subpolar gyre, all models show that UNADW and LNADW transport variability are both strongly and positively correlated with AMOC variability (Figure 4). The UNADW and LNADW correlations with the AMOC are comparable in FLAME (Figure 4a), as expected since the strong subpolar AMOC anomaly in the 1990s appears in both layers (Figures 2b–2d). In ORCA025 and SODA, the correlation between AMOC and UNADW is much stronger than that between AMOC and LNADW (Figures 4b and 4c), suggesting a more dominant role of UNADW in the subpolar gyre on longer time scales (e.g., decadal).

In the subtropical gyre, all models exhibit weak and insignificant correlations between AMOC and UNADW variability at most latitudes. In contrast, LNADW variability is strikingly similar to AMOC variability. Thus, consistent with the RAPID observations, it appears that variability in the lower limb of the AMOC in the

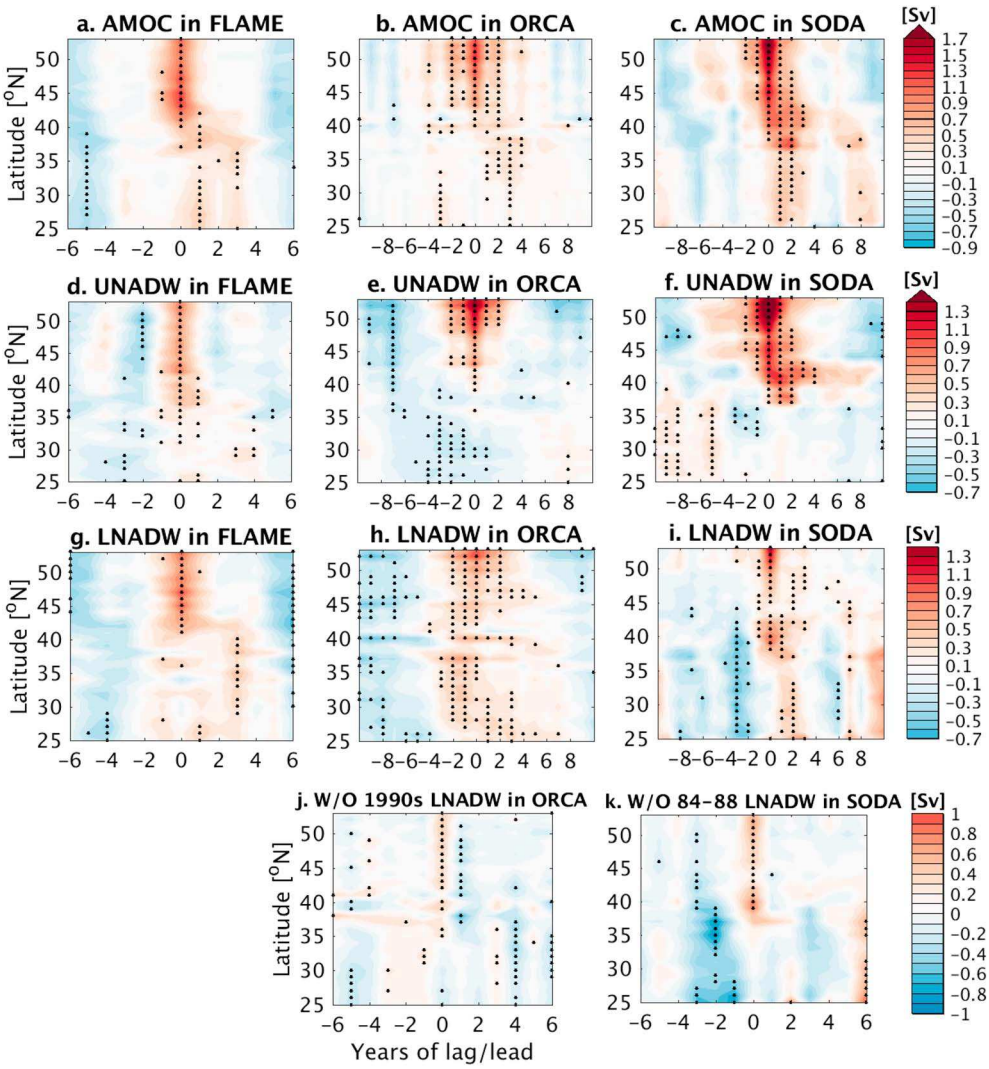

Figure 3. Cross correlation between normalized AMOC time series averaged over 52–53°N and the AMOC time series at other latitudes in (a) FLAME, (b) ORCA025, and (c) SODA. (d–f) Similar to the upper panels, but for UNADW layer transport. (g–i) For LNADW layer transport. (j) For LNADW layer transport in ORCA without the 1990s time series and (k) in SODA without the 1984–1988 time series. During these excluded periods, strong LNADW transport anomalies (exceeding 2 times standard deviation) originate at 52–53°N and propagate to the subtropical gyre within 4 years. Shading indicates the correlation coefficient times the standard deviation of the layer transport at each latitude (unit: Sv). Positive years indicate that the transport at 52–53°N is leading. Black dots indicate correlations significant at a 99% confidence level from Monte Carlo tests. FLAME = Family of Linked Atlantic Models Experiment; UNADW = Upper North Atlantic Deep Water; LNADW = the Lower North Atlantic Deep Water; AMOC = Atlantic Meridional Overturning Circulation; SODA = Simple Ocean Data Assimilation.

subtropical gyre is primarily contained in the LNADW layer. If periods with strong LNADW anomalies are excluded in ORCA (i.e., the 1990s) and SODA (i.e., 1984–1988), such AMOC-LNADW relationship is still significant. This indicates that most of the LNADW anomalies are generated in the subtropical gyre without a subpolar origin and are linked to the same forcing that drives subtropical AMOC variability (e.g., wind forcing, as suggested by Zhao & Johns, 2014). Yeager (2015) suggests that these subtropical LNADW anomalies might be associated with bottom vortex stretching on the continental shelf, in response to winds.

The gyre-dependent relationships between AMOC and UNADW/LNADW transport suggest that the AMOC meridional connectivity may result from a connection between the subpolar UNADW transport and the subtropical LNADW transport. This is especially true in ORCA and SODA, where the dominance of UNADW in

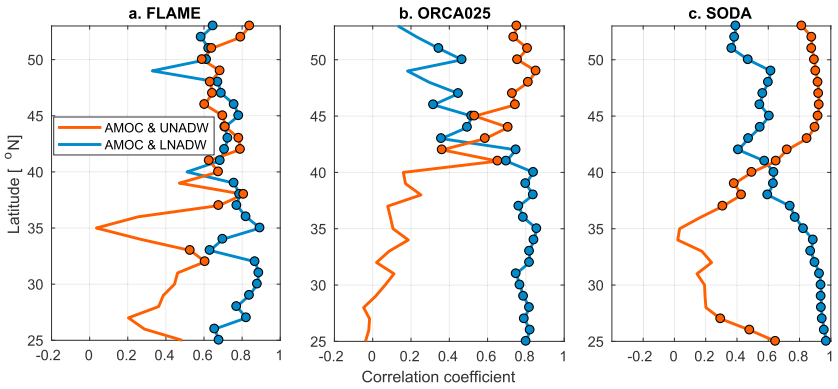

Figure 4. Correlation coefficients between AMOC strength variability and layer transport variability at each latitude in (a) FLAME, (b) ORCA025, and (c) SODA. Colored circles indicate correlations significant at a 99% confidence level. FLAME = Family of Linked Atlantic Models Experiment; UNADW = Upper North Atlantic Deep Water; LNADW = the Lower North Atlantic Deep Water; AMOC = Atlantic Meridional Overturning Circulation; SODA = Simple Ocean Data Assimilation.

the subpolar gyre is more prominent. In support of this argument, an AMOC meridional "connection" is recreated by substituting AMOC with UNADW transport in the subpolar gyre and with LNADW transport in the subtropical gyre within these two data sets. The resultant cross-correlation pattern is very similar to that in Figures 3b and 3c. Such connection is present with or without strong LNADW anomaly periods (Figure S8). A real, rather than an apparent connection, exists only under the conditions of a strong LNADW anomaly, as discussed in section 4.2.

The reason why the subpolar UNADW transport and the subtropical LNADW transport are connected remains unclear. One possibility is that the subpolar UNADW transport is linked to cumulative NAO forcings and the subtropical LNADW transport is associated with individual NAO events. With persistent and strong NAO events, an apparent lagged connection can be established between subpolar UNADW transport anomalies and subtropical LNADW transport anomalies. Another possibility is that the connection is accidental within the time periods addressed here. This is difficult to test given the short time series of high-resolution ocean circulation models.

5. Conclusions

With output from two ocean circulation models and one ocean reanalysis, this study investigates how AMOC meridional connectivity is achieved in density-defined deep layers by focusing on (1) the intragyre connectivity of the transports in deep layers and (2) their linkage to local AMOC strength. It is found that subpolar UNADW transport anomalies are related to local AMOC changes on interannual to decadal time scales, yet these transport anomalies, regardless of strength, do not propagate coherently from the subpolar to the subtropical gyre, nor do they impact the subtropical AMOC strength. These findings challenge the prevailing paradigm that AMOC meridional coherence is achieved via transport in the UNADW layer in response to convective activity in the Labrador Sea.

The lack of meridional coherence in transport anomalies is also evident in the LNADW layer. An exception to this generality is that strong LNADW anomalies are likely communicated to the subtropical gyre, where they have the potential to influence the AMOC strength. Despite this tenuous downstream connectivity for LNADW transport anomalies, a significant linkage between LNADW transport and local AMOC strength is present at all latitudes, and the linkage strengthens from high to low latitudes. In fact, most of the AMOC variability in the subtropical gyre is explained by LNADW transport variability, consistent with observations from RAPID.

Therefore, the AMOC meridional connectivity is not likely to be attributed to a meridional connectivity in either UNADW layer or LNADW layer (except when strong anomalies are present). Instead, the connection is maintained by a lagged correlation between subpolar UNADW transport variability and subtropical LNADW transport variability.

Previous modeling studies have suggested that AMOC meridional coherence between the subpolar and the subtropical gyre is only present under buoyancy forcing, and that such coherence is disturbed when wind forcing is added (e.g., Biastoch et al., 2008; Bingham et al., 2007). However, here we point out that AMOC meridional coherence may also result from forcing scenarios other than that of buoyancy forcing alone. For example, in the early 1990s, though positive buoyancy-forced AMOC anomalies from the subpolar gyre propagate downstream, they are much reduced by the time they reach subtropical latitudes, where much stronger positive wind-forced anomalies are present (e.g., Figure 8 from Biastoch et al., 2008). As such, AMOC can be meridionally connected with gyre-dependent forcing. What remains unclear is how subpolar and subtropical forcing interact to create coherent AMOC/transport anomalies. Insight into this question will be aided by continued observations from the RAPID array as well as those from the recently deployed Overturning in the Subpolar North Atlantic Program (OSNAP; Lozier et al., 2017).

Acknowledgments
The authors gratefully acknowledge support from the U.S. National Oceanic and Atmospheric Administration ESS program (NA16OAR4310168; NA16OAR4310167; awarded to MSL and MB). Gratitude is also extended to C. Böning and A. Biastoch, who graciously shared FLAME and ORCA025 data, and for the open-access SODA data (available at: www.atmos.umd.edu/~ocean/). Data from the RAPID-MOCHA program are funded by the U.S. National Science Foundation and U.K. Natural Environment Research Council and are freely available at www.rapid.ac.uk/rapidmoc and www.rsmas.miami.edu/users/mocha. S. Zou thanks F. Li for codes and helpful discussions on AMOC calculations.

References

Barnier, B., Madec, G., Penduff, T., Molines, J.-m., Treguier, A.-m., Le, J., et al. (2006). Impact of partial steps and momentum advection schemes in a global ocean circulation model at eddy permitting resolution. *Ocean Dynamics*, *56*(5-6), 543–567. https://doi.org/10.1007/s10236-006-0082-1

Biastoch, A., Böning, C. W., Getzlaff, J., Molines, J. M., & Madec, G. (2008). Causes of interannual–decadal variability in the meridional overturning circulation of the midlatitude North Atlantic Ocean. *Journal of Climate*, *21*(24), 6599–6615. https://doi.org/10.1175/2008JCLI2404.1

Bingham, R. J., Hughes, C. W., Roussenov, V., & Williams, R. G. (2007). Meridional coherence of the North Atlantic meridional overturning circulation. *Geophysical Research Letters*, *34*, L23606. https://doi.org/10.1029/2007GL031731

Böning, C. W., Scheinert, M., Dengg, J., Biastoch, A., & Funk, A. (2006). Decadal variability of subpolar gyre transport and its reverberation in the North Atlantic overturning. *Geophysical Research Letters*, *33*, L21S01. https://doi.org/10.1029/2006GL026906

Bower, A. S., Lozier, M. S., Gary, S. F., & Böning, C. W. (2009). Interior pathways of the North Atlantic meridional overturning circulation. *Nature*, *459*(7244), 243–247. https://doi.org/10.1038/nature07979

Cabanes, C., Lee, T., & Fu, L. L. (2008). Mechanisms of interannual variations of the meridional overturning circulation of the North Atlantic Ocean. *Journal of Physical Oceanography*, *38*(2), 467–480. https://doi.org/10.1175/2007JPO3726.1

Carton, J. A., & Giese, B. S. (2008). A reanalysis of ocean climate using Simple Ocean Data Assimilation (SODA). *Monthly Weather Review*, *136*(8), 2999–3017. https://doi.org/10.1175/2007MWR1978.1

Cunningham, S. A., Kanzow, T., Rayner, D., Baringer, M. O., Johns, W. E., Marotzke, J., et al. (2007). Temporal variability of the Atlantic meridional overturning circulation at 26.5°N. *Science*, *317*(5840), 935–938. https://doi.org/10.1126/science.1141304

Delworth, T., Manabe, S., & Stouffer, R. J. (1993). Interdecadal variations of the thermohaline circulation in a coupled ocean-atmosphere model. *Journal of Climate*, *6*(11), 1993–2011. https://doi.org/10.1175/1520-0442(1993)006<1993:IVOTTC>2.0.CO;2

Frajka-Williams, E., Meinen, C. S., Johns, W. E., Smeed, D. A., Duchez, A., Lawrence, A. J., et al. (2016). Compensation between meridional flow components of the Atlantic MOC at 26°-N. *Ocean Science*, *12*(2), 481–493. https://doi.org/10.5194/os-12-481-2016

Gary, S. F., Lozier, M. S., Biastoch, A., & Böning, C. W. (2012). Reconciling tracer and float observations of the export pathways of Labrador Sea Water. *Geophysical Research Letters*, *39*, L24606. https://doi.org/10.1029/2012GL053978

Gary, S. F., Lozier, M. S., Böning, C. W., & Biastoch, A. (2011). Deciphering the pathways for the deep limb of the Meridional Overturning Circulation. *Deep Sea Research Part II: Topical Studies in Oceanography*, *58*(17-18), 1781–1797. https://doi.org/10.1016/j.dsr2.2010.10.059

Goosse, H. (1997). Modeling the large scale behaviour of the coupled ocean-sea ice system. Ph.D. thesis, Université Catholique de Louvain, 231 pp.

Kalnay, E., Kanamitsu, M., Kistler, R., Collins, W., Deaven, D., Gandin, L., et al. (1996). The NCEP/NCAR 40-year reanalysis project. *Bulletin of the American Meteorological Society*, *77*(3), 437–471. https://doi.org/10.1175/1520-0477(1996)077<0437:TNYRP>2.0.CO;2

Lavender, K. L., Owens, W. B., & Davis, R. E. (2005). The mid-depth circulation of the subpolar North Atlantic Ocean as measured by subsurface floats. *Deep-Sea Research I*, *52*(5), 767–785. https://doi.org/10.1016/j.dsr.2004.12.007

Li, F., Lozier, M. S., & Johns, W. E. (2017). Calculating the meridional volume, heat, and freshwater transports from an observing system in the subpolar North Atlantic: Observing system simulation experiment. *Journal of Atmospheric and Oceanic Technology*, *34*(7), 1483–1500. https://doi.org/10.1175/JTECH-D-16-0247.1

Lozier, M. S. (1997). Evidence for large-scale eddy-driven gyres in the North Atlantic. *Science*, *277*(5324), 361–364. https://doi.org/10.1126/science.277.5324.361

Lozier, M. S., Bacon, S., Bower, A. S., Cunningham, S. A., Femke de Jong, M., De Steur, L., et al. (2017). Overturning in the Subpolar North Atlantic Program: A new international ocean observing system. *Bulletin of the American Meteorological Society*, *98*(4), 737–752.

McCarthy, G., Frajka-Williams, E., Johns, W. E., Baringer, M. O., Meinen, C. S., Bryden, H. L., et al. (2012). Observed interannual variability of the Atlantic meridional overturning circulation at 26.5 N. *Geophysical Research Letters*, *39*, L19609. https://doi.org/10.1029/2012GL052933

Polo, I., Robson, J., Sutton, R., & Balmaseda, M. A. (2014). The importance of wind and buoyancy forcing for the boundary density variations and the geostrophic component of the AMOC at 26 N. *Journal of Physical Oceanography*, *44*(9), 2387–2408.

Roberts, C. D., Waters, J., Peterson, K. A., Palmer, M. D., McCarthy, G. D., Frajka-Williams, E., et al. (2013). Atmosphere drives recent interannual variability of the Atlantic meridional overturning circulation at 26.5 N. *Geophysical Research Letters*, *40*, 5164–5170. https://doi.org/10.1002/grl.50930

Schott, F. A., Zantopp, R., Stramma, L., Dengler, M., Fischer, J., & Wibaux, M. (2004). Circulation and deep-water export at the western exit of the subpolar North Atlantic. *Journal of Physical Oceanography*, *34*(4), 817–843. https://doi.org/10.1175/1520-0485(2004)034<0817:CADEAT>2.0.CO;2

Tett, S. F., Sherwin, T. J., Shravat, A., & Browne, O. (2014). How much has the North Atlantic Ocean overturning circulation changed in the last 50 years? *Journal of Climate*, *27*(16), 6325–6342. https://doi.org/10.1175/JCLI-D-12-00095.1

The DRAKKAR Group (2007). Eddy-permitting ocean circulation hindcasts of past decades. *CLIVAR Exchanges*, *12*, 8–10.

Yeager, S. (2015). Topographic coupling of the Atlantic overturning and gyre circulations. *Journal of Physical Oceanography*, *45*(5), 1258–1284.

Yeager, S., & Danabasoglu, G. (2014). The origins of late-twentieth-century variations in the large-scale North Atlantic circulation. *Journal of Climate*, *27*(9), 3222–3247. https://doi.org/10.1175/JCLI-D-13-00125.1

Zhang, R. (2010). Latitudinal dependence of Atlantic meridional overturning circulation (AMOC) variations. *Geophysical Research Letters*, *37*, L16703. https://doi.org/10.1029/2010GL044474

Zhao, J., & Johns, W. (2014). Wind-forced interannual variability of the Atlantic Meridional Overturning Circulation at 26.5° N. *Journal of Geophysical Research: Oceans*, *119*, 2403–2419. https://doi.org/10.1002/2013JC009407

Zou, S., & Lozier, M. S. (2016). Breaking the linkage between Labrador Sea Water production and its advective export to the subtropical gyre. *Journal of Physical Oceanography*, *46*(7), 2169–2182.

Zou, S., Lozier, S., Zenk, W., Bower, A., & Johns, W. (2017). Observed and modeled pathways of the Iceland Scotland Overflow Water in the eastern North Atlantic. *Progress in Oceanography*, *159*, 211–222. https://doi.org/10.1016/j.pocean.2017.10.003